Engineering Structures 195 (2019) 51–61

Contents lists available at ScienceDirect

Engineering Structures

journal homepage: www.elsevier.com/locate/engstruct

Layer model for finite element limit analysis of concrete slabs with shear reinforcement

Thomas Westergaard Jensen[a,b,*], Peter Noe Poulsen[b], Linh Cao Hoang[b]

[a] COWI A/S, Parallelvej 2, Kongens Lyngby, Denmark
[b] Department of Civil Engineering, Technical University of Denmark, Brovej, Building 118, Kongens Lyngby, Denmark

ARTICLE INFO

Keywords:
Limit analysis
Layer model
Concrete slabs
Shear-moment interaction
FELA
Ultimate capacity
Strength-assessment

ABSTRACT

In the last decades, finite element limit analysis has shown to be an efficient method to determine the load-carrying capacity of slab bridges in bending. However, the load-carrying capacity of concrete slabs can be limited by the shear capacity and the redistribution of shear forces when subjected to high-intensity loads such as tire pressure from heavy vehicles. In this paper, an optimised layer model is presented which include limitations on both shear and bending. The layer model is based on a sandwich model, which provides a simple way to determine a safe stress distribution for reinforced concrete slabs with shear reinforcement subjected to shear and bending. The yield criteria in the layer model are formulated as second-order cones which enables an efficient implementation in finite element limit analysis where general convex optimisation algorithms are used. The interaction of section forces is investigated for different combinations of shear forces, moments and torsion. The optimised layer model is used, in combination with finite element limit analysis, to evaluate concrete slabs subjected to different load configurations. The results show that the layer model performs very well with finite element limit analysis and it is possible to determine a safe distribution of shear forces, moments and torsion very efficiently. However, the model cannot handle local effects such as punching shear and concentrated loads near the support.

1. Introduction

The load-carrying capacity of reinforced concrete slab bridges can be limited by the shear capacity and the capability of the structure to redistribute the internal forces. The shear problem arises when heavy vehicles with axle loads are crossing the slab bridges. This is especially critical for wide slab bridges where the redistribution of internal forces is essential for the load-carrying capacity. In practice, the shear problem is often solved by increasing the thickness of the slab to avoid shear reinforcement. However, there can be geometrical constraints fora slab bridge, which limits the thickness. In that case, shear reinforcement, together with redistribution of shear, can be used to increase the load-carrying capacity.

Limit analysis based on the assumption of perfect plastic materials has shown to be an efficient method to determine the load-carrying capacity of reinforced concrete slabs in bending. The most well-known methods are the Yield Line Method [1] and the Strip Method [2]. The yield line method is based on the upper bound theorem and assumes infinite shear capacity. The strip method is based on the lower bound theorem and assumes zero torsional moment which makes it ineffective with respect to redistribution of internal forces.

In the last decades, finite element limit analysis based on the lower bound theorem has shown to be an efficient method to determine the load-carrying capacity of slabs. In the early development, the non-linear yield criteria were linearised [3–5] to enable implementation with the optimisation algorithms for linear programming available at that time. The non-linear convex optimisation algorithms have since been developed, which initiated implementation of non-linear yield criteria [6–8]. For slabs, the conic yield criteria [9] are often used, which can be implemented with second-order cone programming. However, the conic yield criteria only consider bending- and torsional moments.

In recent years, lower bound plate elements which account of shear-bending interaction have been developed. Such an element with a quadratic moment distribution has been implemented with von Mises yield criteria for steel plates [10]. Recently, a lower bound plate element with linear moment distribution has been implemented with the conic yield criteria and with limitations on shear-moment interaction [11]. However, surface loads on the linear element have to be modelled as line loads on the edges of the element. This affects the shear forces in the supported elements, where 1/3 of the load goes directly into the

* Corresponding author at: COWI A/S, Parallelvej 2, Kongens Lyngby, Denmark.
E-mail address: twje@cowi.com (T.W. Jensen).

https://doi.org/10.1016/j.engstruct.2019.05.038
Received 11 February 2019; Received in revised form 9 April 2019; Accepted 13 May 2019

Nomenclature

A_{sx}, A_{sy}	reinforcement area per unit length in the x-and y-direction
A_{sz}	reinforcement area in the z-direction per unit area
c	layer thickness
f_c	compressive strength of concrete
f_y	yield strength of reinforcement
g	general yield criterion
h	height of cross-section
$\boldsymbol{H}$	equilibrium matrix
m_n	moment normal to element edge
m_{nt}	torsional moment normal to element edge
m_{px}, m_{py}	moment capacity about the y- and x-axis
m_x, m_y	moment about the y- and x-axis
m_{xy}, m_{yx}	torsional moment
n_0	normal force in the principal shear force direction
n_x, n_y, n_z	normal force in x-, y- and z-direction
, n_{yx}	in-plane shear force
p	surface load
$\boldsymbol{r}$	load vector
$\boldsymbol{r_c}$	load vector with constant loads
s_x, s_y	stirrup spacing in x- and y-direction
v_0	principal shear force
v_n	shear force normal to element edge
v_{px}, v_{py}	shear capacity in the x- and y-direction
v_x, v_y	shear force in the x- and y-direction
$\boldsymbol{z}$	area coordinate
z_c	position of concrete layer
z_s	position of reinforcement layer
α	auxiliary variable
$\boldsymbol{\beta}$	vector containing all section forces and moments
λ	load factor
μ	coefficient of friction
Φ	reinforcement degree
σ_c	stress in concrete layer
σ_s	stress in reinforcement layer
σ_{xx}, σ_{yy}	normal stress in x- and y-direction
σ_{xy}, σ_{yx}	in-plan shear stress
σ_1, σ_1	largest and smallest principal stress

support.

The shear limitation and shear-bending interaction must ideally be based on a mechanical model, e.g. a sandwich model [12], which is not the case in [11]. In the sandwich model, bending moments and torsional moments are carried by cover layers, and the shear forces are carried by the concrete core layer or shear reinforcement. If the core is not cracked, the shear forces can be carried by the concrete core. If the core is cracked, shear reinforcement carries the shear forces, and the residual concrete shear strength is neglected. In the recent development of the sandwich model, called the extended sandwich model, the aggregate interlock is included in the model. Thus, the concrete contributes to the shear capacity of slabs with as well as without shear reinforcement [13,14]. Another approach to model the shear capacity of slabs with and without shear reinforcement, which has been used with non-finite element analysis, is the multi-layered models [15,16]. In these models, the slab is divided into multiple layers, each of which has a material model, i.e. a model for the stress-strain relationship. The response of the slab is then calculated by integration of the stresses and strains in the layers. Common for the extended sandwich model and the multi-layered model is that they can calculate the shear capacity of slabs with and without shear reinforcement and thus capture brittle shear failures. However, extended sandwich model and the multi-layered models, which utilise the tensile strength of the concrete, cannot be combined with limit analysis which is based on the assumption of perfect plastic material behaviour.

A sandwich model has been developed for a lower bound element to model reinforced concrete shells [17] in which the stresses in the element are limited by the modified Coulomb yield criteria. The shell element consists of three layers in a 3D stress state and is formulated for semi-definite programming [18]. Three layers are, in most cases, not enough to obtain the maximum bending and torsional capacity. Furthermore, semi-definite programming, which is a special type of convex programming, is in general slow compared to conic programming normally used in finite element limit analysis of slabs.

In this paper, an optimised layer model for finite element limit analysis of slabs with shear reinforcement, which includes limitations on moments, torsion and shear forces, is presented. The layer model is based on the concept of the sandwich model [12], where the number of layers, as well as the thickness of each layer, can be optimised to obtain the maximum bending and torsional capacity for orthogonal reinforced slabs. The layer model is implemented in finite element limit analysis of slabs. The implementation of the layer model is done with conic programming which in this case requires a reformulation of the modified Coulomb yield criteria for a 3D stress state. The implementation in conic programming makes the model very efficient with respect to calculation time.

The interactions between bending moments, torsional moments and shear forces are demonstrated with the layer model on different slabs and load configurations. It is shown that the model is capable of handling moment, shear and shear-moment failure. However, the model cannot handle local effects, e.g. punching shear and arch effect near the supports. This is demonstrated with a load on a small area on a large slab. In the example, it is also shown how to detect if a collapse mechanism is due to local effects or not.

In the last example, the layer model is used together with finite element limit analysis to determine the collapse load of a reinforced concrete slab bridge subjected to tire loads at different positions. It is shown that the model can determine the collapse load of the slab with a safe and optimal distribution of stresses for different load configurations very efficiently.

2. Finite element limit analysis of slabs

Finite element limit analysis is a numerical method that combines the discretisation of a structural model, known from the conventional finite element method (FEM), with limit analysis of perfect plastic materials. When applying the lower bound theorem, the objective is to find the maximum load-carrying capacity where the internal stresses and the external loads are in equilibrium, and the stresses are within the yield criteria. The equilibrium can be formulated as

$$\mathbf{H}\boldsymbol{\beta} = \mathbf{r_c} + \lambda\mathbf{r} \tag{1}$$

where $\mathbf{H}$ is the equilibrium matrix, $\boldsymbol{\beta}$ is a vector with all the stress variables, $\mathbf{r_c}$ is a load vector with all the constant loads, and $\mathbf{r}$ is a load vector which is multiplied with the variable load factor λ. The yield criteria can be formulated generally as $g_i(\boldsymbol{\beta}) \leq 0$ for a single or a combination of stress variables. The objective, to maximise the load-carrying capacity, can be obtained by maximising λ. The optimisation problem can be formulated as

$$\begin{aligned} &\text{maximize} && \lambda \\ &\text{subject to} && \mathbf{H}\boldsymbol{\beta} = \mathbf{r_c} + \lambda\mathbf{r} \\ & && g_i(\boldsymbol{\beta}) \leq 0 \quad i = 1, 2...n \end{aligned} \tag{2}$$

where n is the number of yield criteria. These yield criteria are always convex. Thus, the optimisation problem is convex, which always has a unique solution for the maximum load [18].

2.1. Equilibrium conditions for quadratic plate element

A triangular element with quadratic moment distributions is used to discretise the slab model. The element is shown in Fig. 1. The three corner nodes (1–3) and the three nodes on the edges (4–6) define the distribution of bending- and torsional moments. The internal equilibrium in the element is given as

$$\begin{aligned} \frac{\partial v_x}{\partial x} + \frac{\partial v_y}{\partial y} + p &= 0 \\ \frac{\partial m_{xx}}{\partial x} + \frac{\partial m_{yx}}{\partial y} - v_x &= 0 \\ \frac{\partial m_{yy}}{\partial y} + \frac{\partial m_{xy}}{\partial x} - v_y &= 0 \end{aligned} \tag{3}$$

where m_x and m_y are the bending moments, m_{xy} is the torsional moment, v_x and v_y are the shear forces, and p is a surface load. From the internal equilibrium, it is seen that the shear forces can be determined as the partial derivative of the moments. Thus, the shear forces are varying linearly, and the shear force distribution can be established by the use of the three corner nodes (1–3). The shear forces in the side nodes (4–6) are interpolated from the shear forces at the corner nodes. The sectional forces in the internal nodes (7–10) are interpolated from nodes (1–6) and are added to check that the sectional forces in the element are within the yield criteria. The coordinates of the internal nodes, as area coordinates, are

$$\begin{aligned} \mathbf{z}^7 &= \left[\tfrac{1}{3}\ \tfrac{1}{3}\ \tfrac{1}{3}\right],\quad \mathbf{z}^8 = \left[\tfrac{2}{3}\ \tfrac{1}{6}\ \tfrac{1}{6}\right] \\ \mathbf{z}^9 &= \left[\tfrac{1}{6}\ \tfrac{2}{3}\ \tfrac{1}{6}\right],\quad \mathbf{z}^{10} = \left[\tfrac{1}{6}\ \tfrac{1}{6}\ \tfrac{2}{3}\right] \end{aligned} \tag{4}$$

Equilibrium between the elements is obtained at the edges as shown in Fig. 2. The moment m_n, the torsional moment m_{nt} and the shear force v_n are obtained by transformation of the moments and shear forces in the nodes at the edges. The transformation and the equilibrium equations are collected in the equilibrium matrix $\mathbf{H}$ in Eq. (1). A thorough description of the transformation of section forces and the equilibrium between the elements can be found in [19] for a plate element with shear, moment and torsion continuity.

3. Layer model for shear-bending limitations

An optimised layer model for shear-bending limitations in finite element limit analysis is presented in this section. The model is based on the same assumptions used for the well-known sandwich model [12], which has been adopted in the fib Model code [20]. The sandwich model, shown in Fig. 3a, provides a simple way to determine a safe stress state in a slab of a reinforced concrete slab subjected to moments, torsion and shear forces. In the model, it is assumed that the moments and torsion are carried by two reinforced concrete cover layers at the top and bottom of the slab. The shear forces are carried by the reinforced concrete core where a diagonal compression field in the concrete together with tension in the reinforcement ensure equilibrium with the shear actions. Fig. 3b illustrates the diagonal compression field in the core, which is in the direction of the principal stress in the core calculated from the shear forces v_x and v_y together with the forces from the stirrups and the reinforcement in the cover layers.

The bending and torsional capacity depend on the size and number of the cover layers. However, two cover layers are rarely enough to obtain optimality for all four bending capacities and the torsional capacity. If an orthogonal reinforced slab with different amounts of reinforcement in each direction is considered, the optimal size of the cover layer, i.e. the compression zone, will have different sizes for the four optimal bending capacities. The optimal size of the cover layer to obtain maximum torsional moment capacity [9], if the stresses in the cover layer are constant, is given as

$$c_{torsion} = \frac{\Phi_x + \Phi_y}{2} h \tag{5}$$

where $\Phi_x = \frac{\sum A_{sx} f_y}{f_c h}$ and $\Phi_y = \frac{\sum A_{sy} f_y}{f_c h}$ are the reinforcement degrees and h is the total height of the cross-section. Note that the true maximum torsional capacity requires a non-linear stress distribution [21], but the approximation of constant stress zones results in an insignificant smaller capacity. From Eq. (5), it is seen that the optimal size of the compression zone calculated with respect to the torsional capacity only coincides with the optimal size with respect to bending capacity if the slab is isotropic reinforced in the (x, y)-plane and all the reinforcement is yielding at maximum bending. Thus, more cover layers are needed to obtain the maximum moment capacities and the maximum torsional capacity. Furthermore, the concrete and reinforcement also need to be in different layers to get the optimal lever arms for the moment capacities.

The optimised layer model is shown in Fig. 4. The concrete cover layers are divided into multiple layers, which are optimized with respect to the bending and torsional capacities. The concrete and the reinforcement are divided into separate layers to make the size of the concrete cover layers independent of the position of the reinforcement. In this way, the optimised layer model also enables the possibility of more than two reinforcement layers in the (x, y)-plane. Furthermore, the separation of concrete and reinforcement requires individual yield criteria for the materials. Even though this result in more yield criteria, it is considered an improvement compared to the sandwich model. The conic yield criteria for a reinforced concrete disk, which are adopted for the cover layers in the original sandwich model, can overestimate the shear capacity for high reinforcement degrees [22] which lead to an overestimate of the torsional capacity.

The layer model has so far been optimised with respect to the bending and torsional capacities without considering the shear capacities. The optimisation of the bending and torsional capacities can be described as minimisation of the cover layers and maximisation of the lever arm between the concrete in compression and reinforcement in tension. Thus it results in maximisation of the concrete core given maximum bending and torsional capacities. If the total core thickness is maximized with respect to the shear capacities only, the core thickness will be h since an increase of some value k of the core thickness will increase the shear capacities with $\sqrt{k}$ if a constant stress distribution is assumed (This is shown in Eq. (20) in Section 5.1). However, the stirrups need to be able to create compressive stresses in the concrete to carry the shear forces which is a geometric limitation of the core thickness. In this paper, it is assumed that the stirrups can create compression stresses in the concrete which are equivalent to the yield capacity of the stirrups, i.e. the stirrups are perfectly anchored.

The number of core layers is chosen to be one, which limits the distribution of stresses in the whole core to be constant. Such a stress distribution is in most cases not optimal with respect to the shear

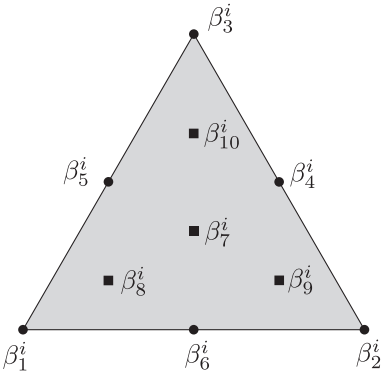

Fig. 1. Quadratic equilibrium slab element. $\beta_j^i = [v_x\ v_y\ m_x\ m_y\ m_{xy}]$ where i is the element number and j is the node number.

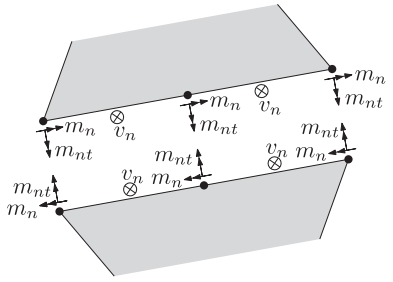

Fig. 2. Equilibrium between element edges.

capacity and shear-bending interaction. However, there exists no specific number of core layers which is optimal since the optimal stress distribution changes due to moments and torsion. The effect of having only one core layer is further addressed in Section 5.1.

In the following, the equilibrium conditions and the yield criteria will be presented for the optimised layer model.

3.1. Equilibrium conditions

The stresses in the concrete and reinforcement layers, shown in Fig. 4, need to be in equilibrium with the sectional forces. The resulting normal forces in a slab are zero, which gives the equilibrium conditions

$$\begin{aligned}
\sum_{i=1}^{n} c_i\sigma_{cx,i} + \sum_{j=1}^{k} A_{sx,j}\sigma_{sx,j} &= n_x = 0\\
\sum_{i=1}^{n} c_i\sigma_{cy,i} + \sum_{j=1}^{k} A_{sy,j}\sigma_{sy,j} &= n_y = 0\\
\sigma_{cz,1} + \sigma_{sz}\tfrac{A_{sz}}{s_x s_y} &= n_z = 0
\end{aligned} \tag{6}$$

where c_i is the thickness of layer i, A_{sx} and A_{sy} are the horizontal reinforcement areas per unit length in layer j, $\sigma_{cx,i}$ and $\sigma_{cy,i}$ are the normal stresses in layer i, $\sigma_{sx,j}$ and $\sigma_{sy,j}$ are the stresses in the reinforcement layer j, $\sigma_{cz,1}$ is the normal stress in the z-direction in the concrete core and σ_{sz} is the normal stress in the stirrups, A_{sz} is the stirrup cross-sectional area and s_x and s_y are the stirrup spacings.

The resulting transverse shear force need to be equal to the sectional shear forces v_x and v_y, and the resulting inplane shear force need to be equal to zero which gives the equilibrium conditions

$$\begin{aligned}
c_1\sigma_{czx,1} &= v_x\\
c_1\sigma_{czy,1} &= v_y\\
\sum_{i=2}^{n} c_i\sigma_{cxy,i} &= n_{xy} = 0
\end{aligned} \tag{7}$$

where v_x and v_y are the transverse shear forces, $\sigma_{czx,1}$ and $\sigma_{czy,1}$ are the transverse shear stresses in the core, and $\sigma_{cxy,i}$ is the shear stress in concrete layer i.

The resulting bending and torsional moments need to be equal to the sectional moments m_x and m_y and sectional torsion m_{xy}, which gives the equilibrium conditions

$$\begin{aligned}
\sum_{i=1}^{n} c_i z_{c,i}\sigma_{cx,i} + \sum_{j=1}^{k} A_{sx,j} z_{s,j}\sigma_{sx,j} &= m_x\\
\sum_{i=1}^{n} c_i z_{c,i}\sigma_{cy,i} + \sum_{j=1}^{k} A_{sy,j} z_{s,j}\sigma_{sy,j} &= m_y\\
\sum_{i=2}^{n} c_i z_{c,i}\sigma_{cxy,i} &= m_{xy}
\end{aligned} \tag{8}$$

where $z_{c,i}$ is the distance from the centre of the section to the centre of concrete layer i, and $z_{sx,j}$ and $z_{sy,j}$ are the distances from the centre of the section to the reinforcement layer j.

3.2. Yield criteria for concrete and reinforcement layers

The reinforcement is modelled as bars which can carry tension forces only. Thus the yield criterion for the reinforcement is given as $0 \le \sigma_s \le f_y$ where σ_s is the stress in the reinforcement bar, and f_y is the yield strength.

The concrete is modelled as a Modified Coulomb material [22] with tensile strength $f_t = 0$. The corresponding yield criteria are shown in Fig. 5a in a σ-τ-system. The yield criteria appear as follows when expressed in terms of principal stresses:

$$\begin{aligned}
\sigma_1 &\le 0\\
k\sigma_1 - \sigma_3 &\le f_c
\end{aligned} \tag{9}$$

where σ_1 is the largest principal stress, σ_3 is the smallest, f_c is the uniaxial compressive strength and $k = (\mu + \sqrt{1+\mu^2})^2$. The coefficient μ for normal strength concrete is often taken as 0.75. Note that the in practice, f_c in the yield criteria must be multiplied with an effectiveness factor $\nu \le 1$ which takes into account the fact that concrete is not a perfectly plastic material [22]. For the sake of simplicity in this paper, ν is set to 1.

The cover layers are assumed to be in a state of plane stress. The modified Coulomb yield criteria for plane stress conditions are shown in Fig. 5b which can be transformed into (σ_{xx}, σ_{yy}, σ_{xy})-space as follows:

$$\begin{aligned}
(-\sigma_{xx})(-\sigma_{yy}) &\ge \sigma_{xy}^2\\
(f_c + \sigma_{xx})(f_c + \sigma_{yy}) &\ge \sigma_{xy}^2
\end{aligned} \tag{10}$$

The concrete core can carry a 3D stress state, where the full yield criteria in Eq. (9) need to be considered. In practice, however, the amount of reinforcement in slabs are rarely large enough to create concrete compressive stresses larger than f_c. It is therefore in most cases only necessary to check if the largest principal stress is $\sigma_1 \le 0$. An exact criterion for when it is only necessary to check the largest principal

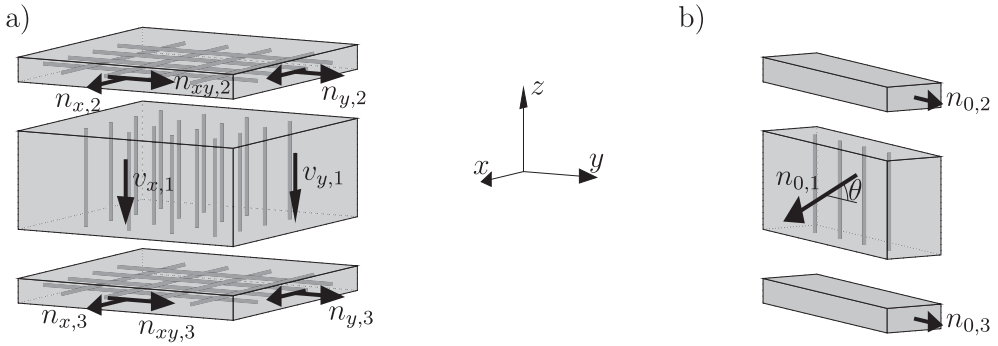

Fig. 3. (a) Sandwich model. (b) Diagonal compression field $n_{0,1}$ in the principal shear v_0 direction.

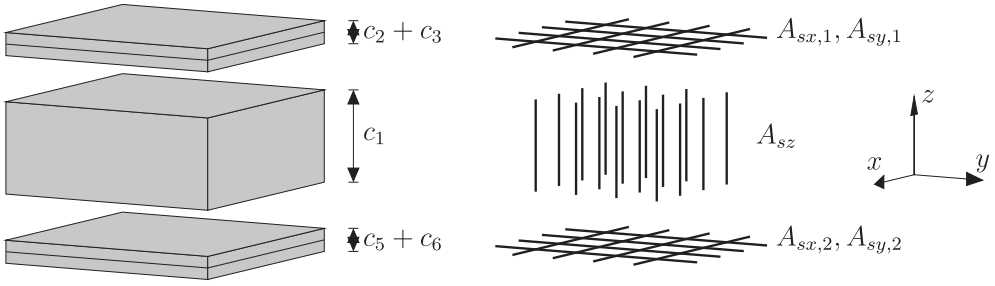

Fig. 4. Example of optimised layer model for numerical limit analysis with one core (c_1), four cover layers (c_2–c_5), stirrups and two layers of reinforcement. (x, y)-plane defines centre plane of slab.

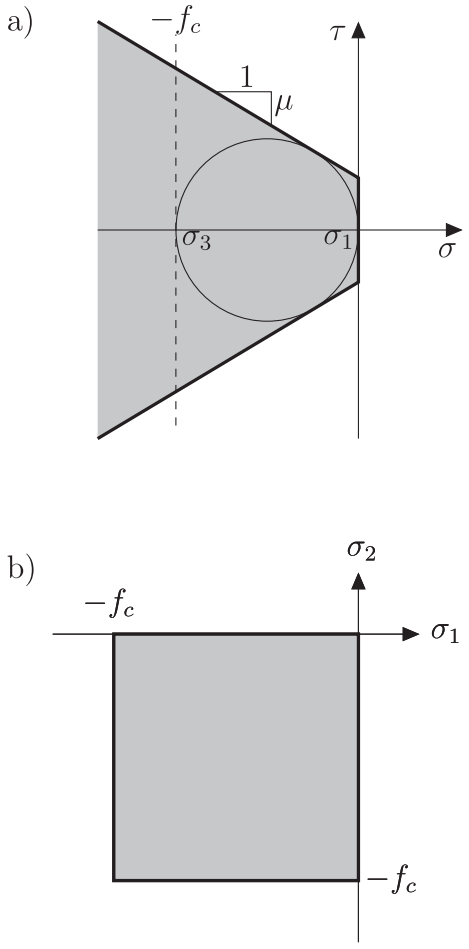

Fig. 5. (a) Modified Coulomb criteria with $f_{ct} = 0$. (b) Modified Coulomb criteria for plane stress conditions.

stress will be derived in Section 4.1 and given in Eq. (19).

4. Implementation of the optimized layer model in finite element limit analysis

The layer models, which account for transverse shear forces, have previously been implemented with semi-definite programming [17]. In this section, an exact implementation with second-order cone programming is presented. Second-order cone programming is a very efficient class of semi-definite programming. Thus the calculation time is reduced by implementation with second-order cone programming.

The equilibrium conditions for the optimised layer model described in Section 3.1 can be implemented as a system of linear equations. The yield criterion for the reinforcement steel is a linear inequality which does not require reformulation to be implemented with second-order cone programming. The yield criteria for the cover layers are formulated directly as second-order cones as shown in Eq. (10). In the following, the implementation of the yield criteria for the core is presented.

4.1. Exact implementation of yield criteria for the concrete core with second-order cones

The concrete core, c_1 in Fig. 4, carries the transverse shear forces by confinement from the reinforcement and stirrups. The horizontal shear stresses σ_{xy} from the torsional moment are zero in the core. The stress tensor for the core is therefore given as

$$\boldsymbol{\sigma} = \begin{bmatrix} \sigma_{xx} & 0 & \sigma_{xz} \\ 0 & \sigma_{yy} & \sigma_{yz} \\ \sigma_{zx} & \sigma_{zy} & \sigma_{zz} \end{bmatrix} \tag{11}$$

where $\sigma_{xz} = \sigma_{zx}$ and $\sigma_{yz} = \sigma_{zy}$. According to the modified Coulomb criteria in Eq. (9), the principal stresses of the stress tensor must be less or equal to zero. The principal stresses are given as the eigenvalues of the stress tensor. Thus, the yield criterion can be formulated as a positive semi-definite inequality given as

$$-\boldsymbol{\sigma} \succeq 0 \tag{12}$$

where "$\succeq$" is the positive semi-definite operator which states that all eigenvalues must be positive or equal to zero.

The stress tensor in Eq. (11) has a Chordal sparsity structure and contains real numbers only. Thus, the positive semi-definite inequality in (12) can be reformulated as

$$-\boldsymbol{\sigma} \succeq 0 \;\Leftrightarrow\; \begin{cases} -\begin{bmatrix} \sigma_{xx} & \sigma_{xz} \\ \sigma_{xz} & \alpha_x \end{bmatrix} \succeq 0 \\ -\begin{bmatrix} \sigma_{yy} & \sigma_{yz} \\ \sigma_{yz} & \alpha_y \end{bmatrix} \succeq 0 \\ \sigma_{zz} = \alpha_x + \alpha_y \end{cases} \tag{13}$$

where α_x and α_y are auxiliary variables. The eigenvalues of a 2×2 symmetric matrix can be formulated as a second-order equation. The semi-definite inequalities in (13) can thus be reformulated as second-order rotated cones given as

$$\begin{aligned} (-\sigma_{xx})(-\alpha_x) &\geq \sigma_{xz}^2 \\ (-\sigma_{yy})(-\alpha_y) &\geq \sigma_{yz}^2 \\ \sigma_{zz} &= \alpha_x + \alpha_y \end{aligned} \tag{14}$$

Note that in standard convex solvers with rotated cones formulated as $x_1 x_2 \geq x_3^2$ it is implicit that $x_1, x_2 \geq 0$. It is therefore not necessary to state the inequalities $-\sigma_{xx} \geq 0$, $-\sigma_{yy} \geq 0$, $-\alpha_x \geq 0$ and $-\alpha_y \geq 0$.

A proof of the reformulation shown in Eq. (13) can be found in [23]. However, it should be noted that the reformulation is only possible if one or more of the shear stresses are zero [24].

The full modified Coulomb yield criteria in Eq. (9) can be formulated as semi-definite inequalities by replacing σ_1 in the second

inequality with an auxiliary variable α_1. The yield criteria are then given as

$$\begin{aligned} &\sigma_1 \le \alpha_1 \le 0 \\ &k\alpha_1 - \sigma_3 \le f_c \end{aligned} \tag{15}$$

Since the stress matrix is symmetric and of real numbers, the eigenvalues can be shifted by adding a constant to the diagonal. Utilising this property, the modified Coulomb yield criteria can be formulated as

$$\begin{aligned} -\boldsymbol{\sigma} + \alpha_1 \boldsymbol{I} &\ge 0 \\ \boldsymbol{\sigma} + (f_c + k\alpha_1)\boldsymbol{I} &\ge 0 \\ \alpha_1 &\le 0 \end{aligned} \tag{16}$$

where $\boldsymbol{I}$ is the identity matrix. The matrices in (16) also have a Chordal structure since σ_{xy} is still zero. Thus, the same reformulation as in (13) can be used on (16), and the modified Coulomb criteria for the core can be formulated as cones given as

$$\begin{aligned} (\alpha_1 - \sigma_{xx})\alpha_2 &\ge \sigma_{xz}^2 \\ (\alpha_1 - \sigma_{yy})\alpha_3 &\ge \sigma_{yz}^2 \\ \alpha_1 - \sigma_{zz} &= \alpha_2 + \alpha_3 \\ (\sigma_{xx} + f_c + k\alpha_1)\alpha_4 &\ge \sigma_{xz}^2 \\ (\sigma_{yy} + f_c + k\alpha_1)\alpha_5 &\ge \sigma_{yz}^2 \\ \sigma_{zz} + f_c + k\alpha_1 &= \alpha_4 + \alpha_5 \\ \alpha_1 &\le 0 \end{aligned} \tag{17}$$

where α_i are auxiliary variables.

The modified Coulomb criteria for the core have been reformulated from two semi-definite inequalities to four conic inequalities. Two of the four cones ensure that the principal stresses are not in tension and two ensure that the principal stresses do not exceed the compression strength. However, it is rarely possible to reach compression stresses up to the compression limit in the core since it is the reinforcement and the stirrups that determine the maximum possible stresses. The maximum normal compression stresses in the core are given as

$$\sigma_{xx,max} = -\Phi_x \frac{h}{c_1} f_c, \quad \sigma_{yy,max} = -\Phi_y \frac{h}{c_1} f_c, \quad \sigma_{zz,max} = -\Phi_z f_c \tag{18}$$

where $\Phi_x = \frac{\sum A_{sx} f_y}{f_c h}$ and $\Phi_x = \frac{\sum A_{sy} f_y}{f_c h}$ are the reinforcement degrees, $\Phi_z = \frac{A_{sx} f_y}{f_c s_x s_y}$ is the stirrup degree with the stirrup spacing s_x and s_y, and c_1 is the thickness of the core. In Eq. (17) it is seen that the minimum compression strength occurs when $\alpha_1 = 0$, i.e. at plane stress state with the compression strength f_c. Inserting the maximum compression stresses from Eq. (18) in the modified Coulomb yield criteria for plane stress in Eq. (10), the limit for when it is not necessary to check the compression strength can be found as

$$\max(\Phi_x, \Phi_y)\frac{h}{c_1} + \Phi_z \le 1 \tag{19}$$

It can be concluded that the yield criteria for the core can be implemented with Eq. (14) if the inequality (19) holds. Otherwise, the yield criteria must be implemented by the use of Eq. (17).

5. Numerical examples

The layer model presented in Section 3 has been implemented with numerical limit analysis as described in Section 2. The implementation is made according to Section 4. In the following examples, a slab element with isotropic reinforcement in the (x,y)-plane is used to determine the yield surfaces obtained by the layer model. Furthermore, it will be shown how the layer model performs with finite element limit analysis. If nothing else is stated, the cross-sectional properties shown in Table 1 is used. With these properties, one cover layer in the top and bottom is optimal with a thickness of $c_2 = c_3 = 0.05$ m and the core thickness is $c_1 = 0.4$ m.

5.1. Layer model

A layer model of a slab unit, as shown in Fig. 4, is analysed to demonstrate the moment, torsion and shear capacities as well as the interaction of section forces. The cover layers are optimised with respect to the bending- and torsional capacities.

The conventional yield criteria for slabs in bending are the conic yield criteria [9]. The assumptions for the conic yield criteria are the same as for this layer model when shear forces are neglected. The yield surfaces calculated with the layer model are shown in Fig. 6 for the case $v_x = v_y = 0$. It is seen that the layer model produces two cones, which are identical with the conic yield criteria. However, it should be noted that the yield surface produced by the layer model and the conic yield criteria only coincide if both layers of reinforcement yield at maximum bending moment as they do for maximum torsional moment. In any other cases, the yield surface of the layer model will be within the conic yield criteria since the latter overestimates the torsional capacity [22].

For one-way bending, the interaction between moment capacity and shear capacity can be calculated analytically for the presented layer model with one core layer and isotropic reinforcement in the (x,y)-plane. The moment capacity m_{px} is a linear function of the amount of reinforcement A_{sx}. From Eq. (10), the shear capacity v_{px} can be formulated as

$$v_{px} = \sqrt{\sigma_x \sigma_z}\, c_1 = \sqrt{\frac{\sum A_{sx} f_y}{c_1} \frac{A_{sz} f_y}{s_x s_y}}\, c_1 \tag{20}$$

where c_1 is the thickness of the core shown in Fig. 4. Note that Eq. (20) is similar to the shear capacity of a reinforced concrete disk [22]. Eq. (20) shows that v_{px}^2 is a linear function of A_{sx}. Hence, the moment capacity m_{px} as a function of the shear force v_x can be formulated as

$$m_{px}(v_x) = m_{px,0}\left(1 - \left(\frac{v_x}{v_{px,0}}\right)^2\right) \tag{21}$$

where $m_{px,0}$ is the moment capacity for pure bending and $v_{px,0}$ is the shear capacity for pure shear. The same result was obtained in [25]. The shear-bending interaction in Eq. (21) is only optimal for the layer model with one core layer and reinforcement with the same centroid as the core layer. The optimal stress distribution in the core with respect to the shear capacity becomes non-linear when a moment m_x is acting on the cross-section, or the centroid of the reinforcement does not coincide with the centroid of the core. Thus the maximum shear capacity cannot be obtained with one or more core layers with a constant stress distribution. In Fig. 7, the reduction due to the few core layers with constant stress distributions is shown as a function of the relative centroid of the reinforcement $\frac{e_s}{e_c}$. If $\frac{e_s}{e_c} = 1$ the reinforcement and the concrete core have the same centroid. It is seen that one core reduces the shear capacity significantly more than two or three cores. Hence, more than one core layer increases the shear capacity in most cases. However, when choosing the number of core layers, the computational time must also be considered. An extra core layer adds four conic constraints at every node as shown in Eq. (17). In the following, the layer model with one core layer is still considered.

The interaction between the torsional capacity and the shear forces

Table 1
Cross-sectional properties of slab.

Height, h	0.5	[m]
Concrete strength, f_c	45	[MPa]
Reinforcement degree, $\Phi_x = \Phi_y$	0.1	[–]
Stirrup degree, Φ_z	0.1	[–]
Reinforcement cover	0.05	[m]

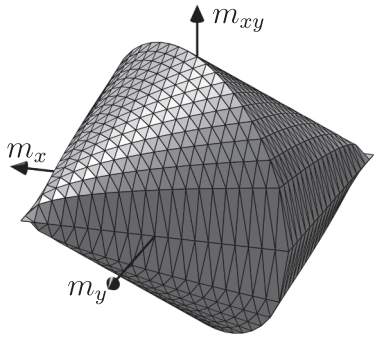

Fig. 6. Yield surfaces for combinations of (m_x, m_y, m_{xy}) with $v_x = v_y = 0$.

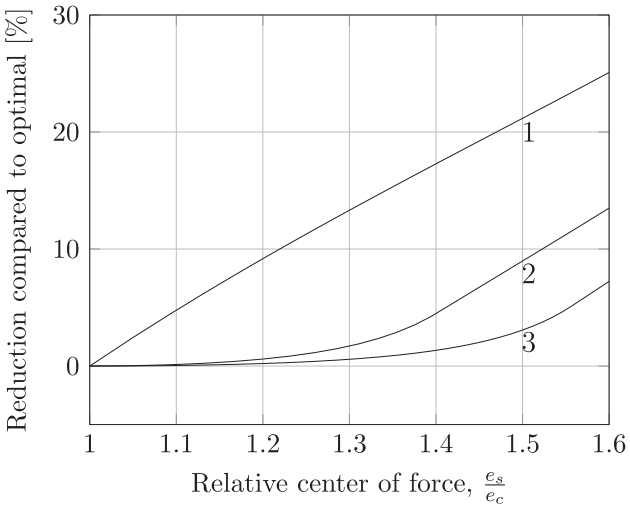

Fig. 7. Reduction of pure shear strength for layer models with 1, 2 and 3 core layers compared to shear strength with optimal stress distribution. The minimum principal stress is assumed to be $\sigma_3 \geq -f_c$. e_c is the centroid of the total core, and e_s is the centroid of the reinforcement.

is shown in Fig. 8. The shear forces in both directions affect the torsional capacity since reinforcement in the x- as well as the y-direction is needed to carry the torsional moment. The figure shows that the combined shear capacity can be formulated as a second-order inequality $\left(\frac{v_x}{v_{px}(0)}\right)^2 + \left(\frac{v_y}{v_{py}(0)}\right)^2 \leq 1$ when the torsion is zero. When the torsional moment increases towards the maximum torsional capacity, the combined shear capacity approaches a linear inequality formulated as $\frac{v_x}{v_{px}(m_{xy})} + \frac{v_y}{v_{py}(m_{xy})} \leq 1$. Thus the maximum possible principal shear force is in the x- or y-direction, i.e. the directions of the reinforcement, when the torsional moment increases towards the maximum torsional capacity.

5.2. Quadratic element

The moment distribution in the element shown in Fig. 1 is quadratic. Thus, the maximum moments can occur anywhere on the element and not just at the corner and side nodes (1–6) as for a linear element. Extra nodes in the centre (nodes 7–10 on Fig. 1) are added to ensure that the section forces are within the yield criteria at these nodes as well. The sectional forces and moments in the centre nodes are interpolated from the nodes at the corner and edges. In Fig. 9, the maximum moment is shown for an element with no centre node, one centre node and three centre nodes. The moment is limited by the yield criterion $-1 \leq m \leq 1$ at the nodes.

The figure shows that if the yield criteria are not checked in the centre of the element, the moment can be overestimated by 67%. If one or four nodes are placed in the centre, the overestimates are 33% and 25% respectively. However, the variation of the moment in the element is very large for all cases which can result in large shear forces according to the equilibrium Eqs. (3). Furthermore, these extreme variations of moments within an element are rarely the optimal distribution for a slab discretised by many elements as is shown in the next example.

5.3. Clamped square slab

The clamped square slab with uniform surface load is a benchmark example for convergence test in finite element limit analysis of slabs in bending. The exact solution is $p = 42.851\frac{m_p}{l^2}$[26] when the conic yield criteria for isotropic reinforced slabs are used [9]. In the previous section, it is shown that the optimised layer model coincides with the conic yield criteria for specific cross-sections. Thus the layer model implemented in finite element limit analysis can be compared with the analytic solution for bending where shear forces are not considered. The results obtained by the use of elements with 6, 7 and 10 nodes are shown in Fig. 10. The figure shows that the element with 10 nodal checkpoints converges from a lower value than the exact one. The elements must converge from a lower value to be a true lower bound element. The elements with 6 and 7 nodal checkpoints can overestimate the capacity. However, the overestimates are very small compared with the maximum possible violation of the yield criteria for the elements shown in Fig. 9 and they are decreasing with an increasing number of elements.

The yield criteria for each layer in an optimised layer model are checked at every node in the element. Hence, the extra nodes result in extra computation time. For a dense mesh, the elements with 6 or 7 nodes are therefore preferred since the calculations still lead to

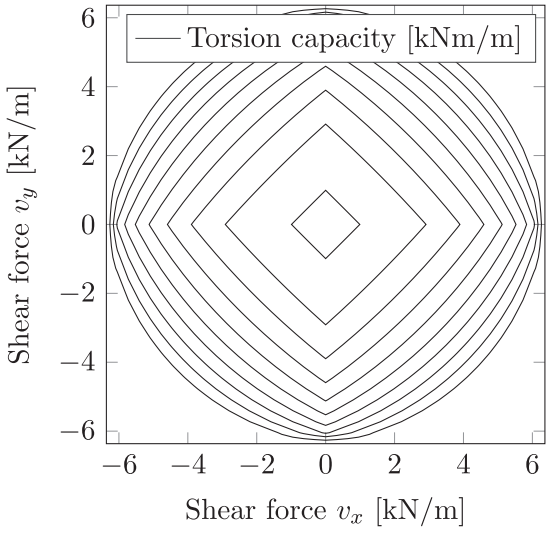

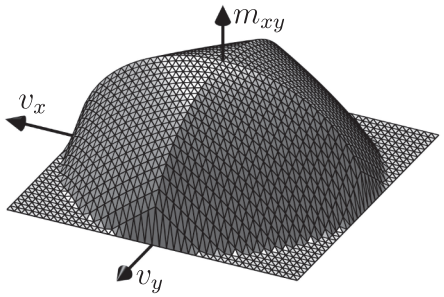

Fig. 8. Yield surface of torsion and shear forces only. Contour line spacing: 50 [kN m/m].

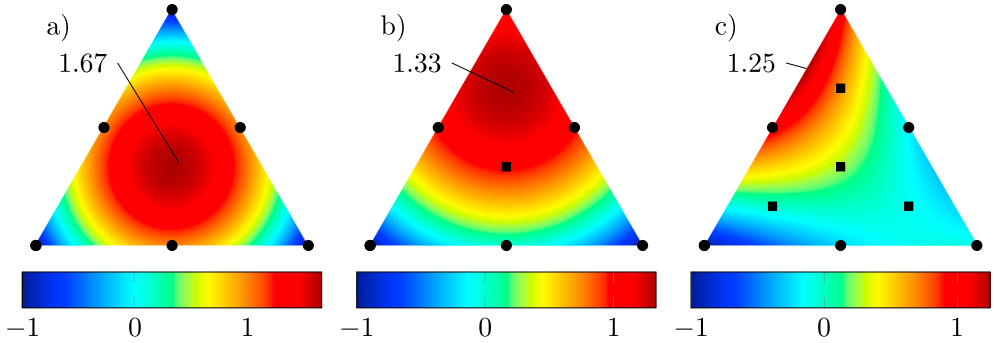

Fig. 9. Maximum possible moment in element with quadratic moment distribution. Moment limitation at control points: $-1 \leq m \leq 1$. (a) 6 control points, $m_{max} = 1.67$. (b) 7 control points, $m_{max} = 1.33$. (c) 10 control points, $m_{max} = 1.25$.

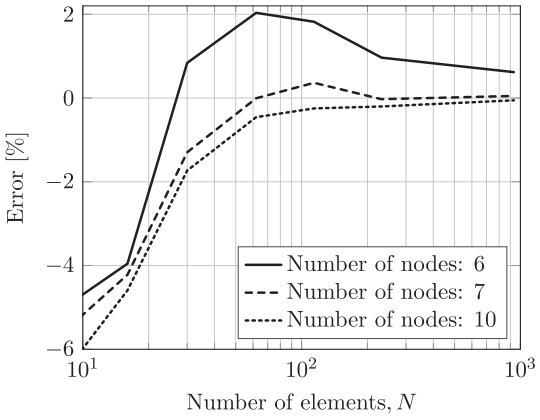

Fig. 10. Convergence of a clamped square slab with a uniform load. Analytical solution: $p = 42.851\frac{m_p}{l^2}$.

sufficient accurate results as shown in Fig. 10. It should be noted that all computation times for the clamped square slab are within seconds.

5.4. Cantilever slab subjected to a single load

The capability to limit the shear forces is demonstrated with a cantilever slab subjected to a single load, as shown in Fig. 11. The slab is analysed with different amounts of shear reinforcement. To ensure a shear failure, the degree of reinforcement in the span direction is increased to $\Phi_x = 0.6$, while the other material parameters are shown in Table 1.

The results are shown in Fig. 11. If the shear forces are not limited, the load-carrying capacity increases towards infinity for a decreasing distance from the load to the support which is not the case for the model with shear limitations. For the slab with the lowest amount of shear reinforcement, the load-carrying capacity is constant for the load placed at $x = 0$ to $x = 1.4$ m. This is due to the compressive strength of the core, which is reached to carry the shear forces. After $x = 1.4$ m, the load-carrying capacity decreases due to an increasing moment and a decreasing compression in the core. As the distance from the load to the support increases, the load-carrying capacity of the model with shear limitations is approaching the load-carrying capacity of the model without shear limitation.

The same behaviour is seen for the slab with a shear reinforcement degree of $\Phi_z = 0.1$. However, the magnitude and position of the load where the load-carrying capacity starts to decrease are different. Because of the high reinforcement degree in the span direction, the load-carrying capacity will increase with an increasing shear reinforcement degree until $\Phi_z = \frac{1}{2} - \frac{k\sigma_1}{2f_c}$.

5.5. Slab subjected to a concentrated load

In this section, load configurations with a single concentrated load on a simply supported single span wide slab are analysed to investigate when the local effects dominate the load-carrying capacity. The cross-sectional properties used in the analyses are shown in Table 1. The slab spans 5 m and is 5 m wide. The element, shown in Fig. 1, is used for the analysis with one centre node and a size of 0.1 m.

The slab is analysed with varying size of the square loading area in the centre of the slab. The results are shown in Fig. 12 for three different shear capacities. It is seen that the same capacity is obtained for the case with infinite shear capacity and the two cases with limited shear capacity for load sizes of 0.6–2 m. In this range, failure of the slab is dominated by bending for all cases. Approximately the same results can be obtained with the yield line method or finite element limit analysis with the conic yield criteria. However, these methods do not ensure that the slab does not fail in shear.

The failure mode can be interpreted from the collapse mechanism which is extrapolated from the dual variables (see [11]). The collapse mechanism along the centre line of the slab is shown in Fig. 13. The figure shows that a plastic hinge has been developed in the middle of the span for $a = 0.6$. In this case, the whole slab is failing in bending. A second failure is shown in the figure for $a = 0.2$ where the load-carrying capacity is decreasing at a very fast rate due to a decrease in the loading area. It is seen that the failure, in this case, is concentrated around the loaded area where there is a vertical drop. The failure is local which in the context of the present model may be interpreted as a shear/punching shear failure. In reality, however, punching shear failures are always associated with formations of diagonal cracks around the loaded area [27] which activate the stirrups crossing the cracks. The punching

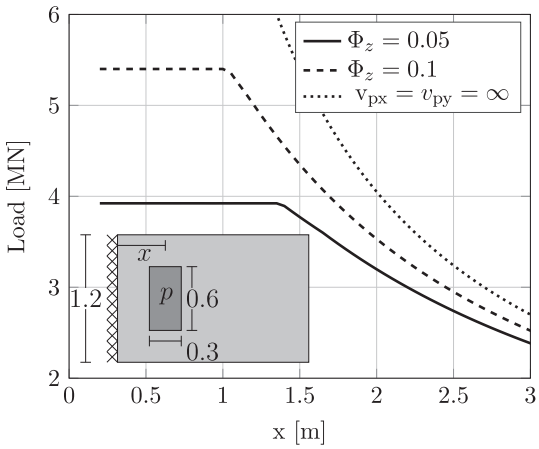

Fig. 11. Load carrying-capacity of cantilever slab subjected to the surface load p. All dimensions are in [m]. The reinforcement degree Φ_x is increased to 0.6.

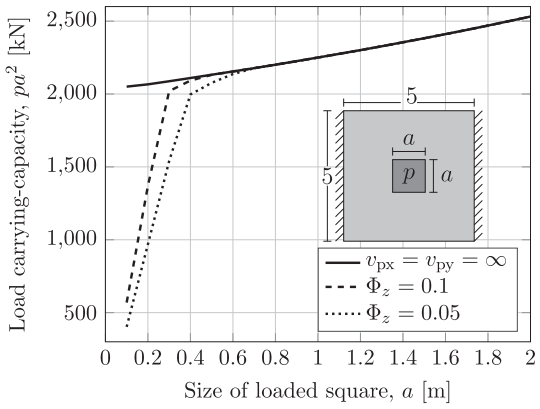

Fig. 12. Load carrying-capacity of a square slab with a square loading area in the centre of varying size. All dimensions are in [m].

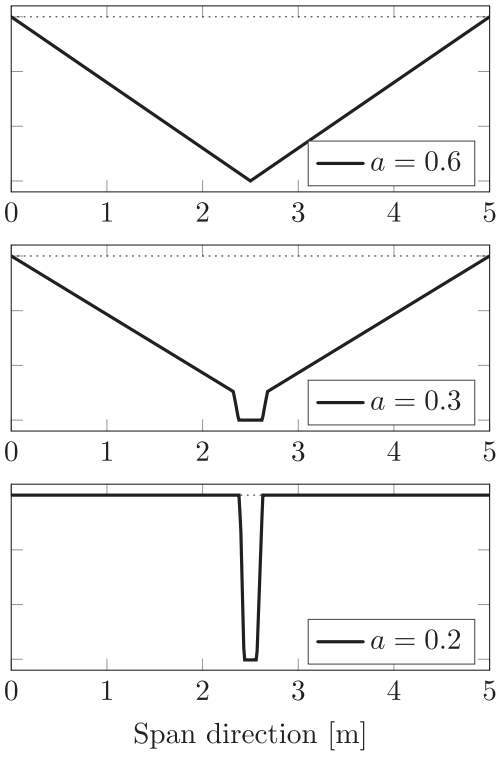

Fig. 13. Collapse mechanism along the centre line in span direction for the example shown in Fig. 12. a [m] is the size of the square load and. $\Phi_z = 0.1$.

shear capacity due to failure in diagonal cracks can be calculated using the theory of rigid plasticity [22,28]. As a consequence of the Coulomb material model for concrete and the normality condition of plastic theory, the horizontal projection of the diagonal cracks is at least $0.75h$ [22]. If the contribution from the concrete is neglected and if it is assumed that the stirrups are closely spaced, the minimum punching shear capacity can then be estimated as

$$P_{min} = \Phi_z f_c \left(4 \cdot 0.75ha + (0.75h)^2 \pi\right) \tag{22}$$

where a is the size of the square load. The minimum punching shear capacity of the slab with the properties in Table 1 and the load size $a = 0.2$ is 3338 kN. The results of the layer model, shown in Fig. (12), is 1370 kN for the load size $a = 0.2$, where a failure equivalent to the punching shear failure occurred. The difference between the two calculations clearly shows the limitation of the layer model combined with finite element limit analyse of slabs where sectional shear forces and moments are limited at each point by the yield criteria. However, the

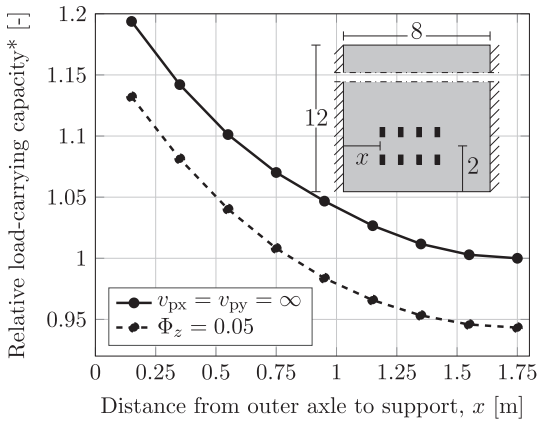

Fig. 14. Load carrying-capacity of bridge subjected to moving axle loads. All dimensions are in [m]. (∗) The relative load-carrying capacity is relative to the load-carrying capacity of the axles placed in the centre of the span ($x = 1.75$) and $v_{px} = v_{py} = \infty$.

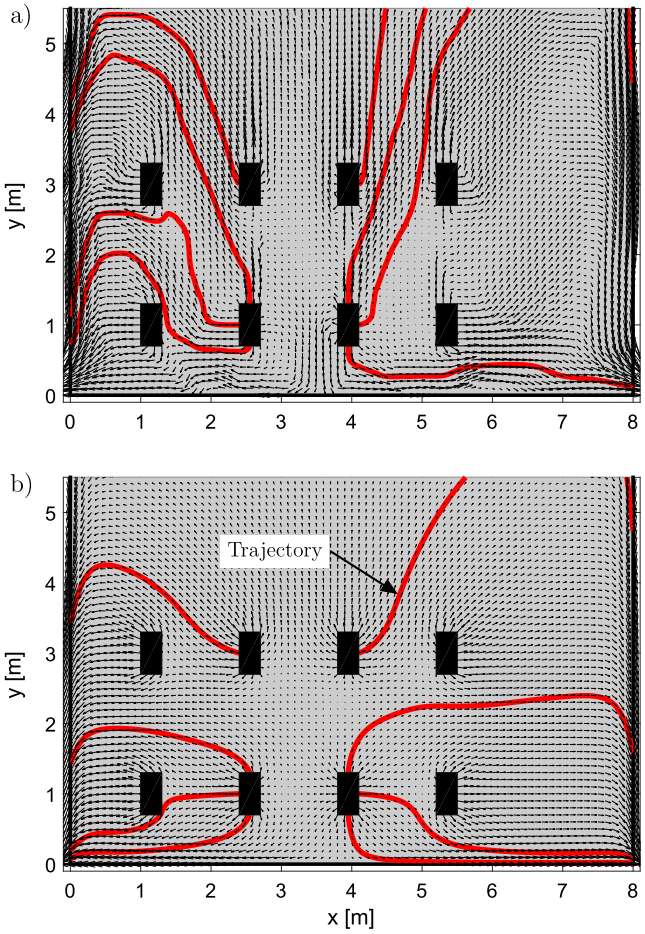

Fig. 15. Shear force distribution. The direction of the arrows is $\arctan\frac{v_y}{v_x}$, and the length is $v_0 = \sqrt{v_x^2 + v_y^2}$. The lines are calculated trajectories (streamlines). (a) Finite element limit analysis. (b) Linear elastic finite element analysis.

presented model considers shear-moment action in the whole slab at the same time while a local punching shear calculation only considers one failure mode. Hence, the model can redistribute the forces but cannot capture local failure mechanisms. A common practical solution to calculate the punching shear capacity with sectional analysis is to check the shear forces at a nominal distance from the concentrated load

Table 2
Comparison of calculation time for conic and semi-definite implementation of the core layer. Bridge example in Fig. 14 with the load in the centre.

No. of elements	2 516	5 598	9 960	22 342
Conic [s]	16.7	40.2	72.2	178
Semi-definite [s]	25.5	61.3	105	253
Conic/Semi [–]	0.65	0.66	0.69	0.70

and not at the edge of the load. This approach is not treated further in this paper.

5.6. Slab bridge subjected to four moving axle loads

To demonstrate the practical application of the layer model implemented in finite element limit analysis, a slab bridge subjected to four moving axle loads is analysed. The moving loads require multiple calculations to find the most critical position of the loads. Thus, a time-efficient calculation method is required.

In practice, the standards have additional limitations to the concrete strength and the stress-state in the slab which are not accounted for in the analysis. For example, the angle between the minimum principal stress and the (x, y)-plane must be within a certain interval [29,20]. These additional limitations are not within the scope of this paper and require further development to be implemented.

The dimensions of the bridge are shown in Fig. 14. The four axles represent the heavy rear axles of a truck. The contact area of the tires is 0.3×0.6 m. The width of the axles is 2.8 m, and the distance between the axles is 1.4 m. All the dimensions are according to the Danish standard [30].

In the analyses, 5600 7-node elements are used, and the Mosek [31] software package for Matlab is used to solve the optimisation problem. The total calculation time on a standard laptop for each load position is within 1 min for the full layer model.

The results are shown in Fig. 14. When $x = 1.75$, the axles are placed at the centre of the span. At this position, the load-carrying capacity for $\Phi_z = 0.05$ is 6% smaller than the analysis where the shear capacity is neglected. The figure shows that the difference remains the same as the axles moving towards the support. This indicates that the shear forces are not critical for the load-carrying capacity of the bridge.

The shear force distribution of the optimal solution for the axle loads placed $x = 1.0$ m from the support is shown in Fig. 15a. The direction of the arrows with respect to the x-axis is $\arctan\frac{V_y}{V_x}$. To evaluate the extent of redistribution of internal forces, the shear distribution is compared with a linear elastic finite element analysis. In the analysis, the properties, shown in Table 1, is used with triangular Reissner–Mindlin elements with quadratically shape functions [32]. The shear force distribution of the analysis is shown in Fig. 15b. To compare the flow of shear forces, trajectories starting from the inner axle loads are calculated and drawn in the figures with red lines. The figures show that the shear forces obtained from the limit analysis are further distributed into the slab compared with the linear elastic analysis. This is especially seen from two of the trajectories at the load at the coordinate (4,1) where shear forces obtained from the limit analysis are primarily directed in the y-direction and shear forces obtained from the linear elastic analysis are approximately directed in the x-direction. The increase of the load-carrying capacity due to the optimal redistribution of internal forces is, for this example, 47%.

It should be noted that the shear force distribution of the optimal solution shown in Fig. 15a is not unique. In the part of the slab where the internal forces and moments are not on the yield surface, the optimisation algorithm can choose any shear force distribution which is admissible and does not interfere with the optimal solution.

5.7. Calculation time

The efficiency of the implementation of the layer model in finite element limit analysis is analysed. The core layer is implemented with the conic constraints shown in Eq. (14) and with a semi-definite constraint shown in Eq. (12) for comparison. The bridge example in Fig. 14 with the load placed in the centre (x = 1.75 m) is used for the analysis. The results are shown in Table 2 for a different number of elements. The load carrying capacity is the same for all calculation which indicates that the solution has converged even for the smallest number of elements. The table shows that the model with the core layer implemented with conic constraints is approximately 50% faster than the model with the core layer implemented with a semi-definite constraint.

6. Conclusion

An optimised layer model has been presented which can handle bending moments, torsional moments and shear limitations in reinforced concrete slabs. Contrary to the well-known sandwich model, the layer model divides the slab into separate concrete and reinforcement layers, which have individual yield criteria. This ensures that the torsional capacity is not overestimated which will be the case if heavily reinforced slabs are modelled with the sandwich model.

The interaction of section forces has been demonstrated. It has been shown that the layer model can produce the same yield surface as the conic yield criteria when bending and torsional moments are considered for a slab with isotropic reinforcement in the (x, y)-plane. The interaction between shear forces shows that the shear capacity is constant if no other section forces or moments are acting on the cross-section. However, when a torsional moment is acting on the cross-section, the interaction between the shear forces v_x and v_y in the layer model with one core becomes linear for increasing torsional moments.

The optimised layer model has been implemented with finite element limit analysis. The yield criteria for the core have been reformulated so that the model can be implemented with second-order cone programming. For the case analysed, this implementation results in approximately 50% faster calculation time than an implementation with semi-definite constraints.

It has been demonstrated that the model can handle both moment, shear and shear-moment failure. However, the model cannot handle local effects such as punching shear and concentrated loads near the support. It has been shown that the failure mechanisms can be used to determine when these effects dominate the load-carrying capacity and additional analysis is required to get the optimal load-carrying capacity.

As a practical example, the load-carrying capacity of a bridge subjected multiple moving axle loads. The model takes into account shear-bending actions and redistribution of internal forces. However, additional limitations on the concrete strength and stress-state, which the standards require, are not considered in the examples and need further development to be implemented.

Acknowledgement

The work described in this paper was financially supported by COWIfonden, Innovation Fund Denmark (Grant No. 5190-00036B) and the Danish Road Directorate.

References

[1] Johansen KW. Brudlineteorier (English translation: Yield Line Theory). Gjellerups Forlag 1943;1943.
[2] Hillerborg A. Strip method of design, no. Monograph, 1974; 1974.
[3] Anderheggen E, Knöpfel H. Finite element limit analysis using linear programming. Int J Solids Struct 1972;8(12):1413–31.
[4] Chan HSY. The collapse load of reinforced concrete plate. Int J Numer Meth Eng 1972;5(1):57–64.
[5] Faccioli E, Vitiello E, element A finite. linear programming methods for the limit

analysis of thin plates. Int J Numer Meth Eng 1973;5(3):311–25.
[6] Krabbenhøft K, Damkilde L. Lower bound limit analysis of slabs with nonlinear yield criteria. Comput Struct 2002;80(27):2043–57.
[7] Krabbenhøft K, Lyamin AV, Sloan SW. Formulation and solution of some plasticity problems as conic programs. Int J Solids Struct 2007;44(5):1533–49.
[8] Nielsen LO, Poulsen PN. Computational limit analysis of perfectly plastic plate bending based on lower bound optimization. DSBY 2009:67–115.
[9] Nielsen MP. Flydebetingelser for jernbetonplader (English summary: yield conditions for reinforced concrete slabs). Nordisk Betong 1963:61–82.
[10] Bleyer J, Buhan PD. Lower bound static approach for the yield design of thick plates. Int J Numer Meth Eng 2014;100(11):814–33.
[11] Jensen TW, Poulsen PN, Hoang LC. Finite element limit analysis of slabs including limitations on shear forces. Eng Struct 2018;174:896–905.
[12] Marti P. Design of concrete slabs for transverse shear. Struct J 1990;87(2):180–90.
[13] Jaeger T. Extended sandwich model for reinforced concrete slabs: Shear strength without transverse reinforcement. Eng Struct 2013;56:1142–53.
[14] Jaeger T. Extended sandwich model for reinforced concrete slabs: shear strength with transverse reinforcement. Eng Struct 2014;74(2014):218–28.
[15] Polak MA, Vecchio FJ. Nonlinear analysis of reinforced-concrete shells. J Struct Eng 1993;119(12):3439–62.
[16] Hrynyk TD, Vecchio FJ. Capturing out-of-plane shear failures in the analysis of reinforced concrete shells. J Struct Eng 2015;141(12):4015058.
[17] Larsen KP, Poulsen PN, Olesen JF. Numerical limit analysis of reinforced concrete structures: computational modeling with finite elements for lower bound limit analysis of reinforced concrete structures Ph.D. thesis Technical University of Denmark (DTU); 2011.
[18] Boyd S, Vandenberghe L. Convex optimization. Cambridge University Press; 2004.
[19] Jensen TW, Poulsen PN, Hoang LC. Numerical lower bound analysis of plate bending problems containing requirements on shear capacity and shear-bending interaction. In: Computational modelling of concrete structures; 2018. p. 625–32.
[20] Fédération Internationale Du Béton, Model Code 2010, fib Bulletins 65 & 66, Lausanne, 2012; 2012.
[21] Marti P. Zur plastischen Berechnung von Stahlbeton, Ph.D. thesis; 1980.
[22] Nielsen MP, Hoang LC. Limit analysis and concrete plasticity. CRC Press; 2011.
[23] Vandenberghe L, Andersen MS. Chordal graphs and semidefinite optimization. Found Trends Optimiz 2015;1(4):241–433. https://doi.org/10.1561/2400000006. URL http://www.nowpublishers.com/article/Details/OPT-006.
[24] Fawzi H. On representing the positive semidefinite cone using the second-order cone; 2016. arXiv preprint arXiv: 1610.04901.
[25] Grob J, Thürlimann B. Ultimate strength and design of reinforced concrete beams under bending and shear. Ultimate strength and design of reinforced concrete beams under bending and shear/Résistance et dimensionnement des poutres en béton armé soumises à la flexion et à l'effort tranchant/Bruchwiderstand und Bemessung von Stahlbetonbalken unter Biegung und Sc. Springer; 1976. p. 107–20.
[26] Fox EN. Limit analysis for plates: the exact solution for a clamped square plate of isotropic homogeneous material obeying the square yield criterion and loaded by uniform pressure. Philos Trans R Soc Lond A: Math Phys Eng Sci 1974;277(1265):121–55.
[27] Lips S, Fernández Ruiz M, Muttoni A. Experimental investigation on punching strength and deformation capacity of shear-reinforced slabs. ACI Struct J 2012;109:889–900. URL https://infoscience.epfl.ch/record/181777.
[28] Hoang LC, Pop A. Punching shear capacity of reinforced concrete slabs with headed shear studs. Mag Concr Res 2015. https://doi.org/10.1680/macr.15.00033http://orbit.dtu.dk/ws/files/111902817/macr_punching_Hoang_Pop_2015_.pdf.
[29] Dansk standard. Eurocode 2: design of concrete structures – Part 1-1: general rules and rules for buildings, 3rd ed.; 2008.
[30] Vejdirektoratet. Annex A (Normative) Lastmodeller for klassificering og bæreevnevurdering; 2013.
[31] M. ApS. The MOSEK optimization toolbox for MATLAB manual. Version 8.1.; 2017. http://docs.mosek.com/8.1/toolbox/index.html.
[32] F.E.A. DIANA. Diana User's Manual, Release 10.2; 2017.